Application News

AGX™-V Precision Universal Testing Machine, HMV™-G31-FA Series Micro Vickers Hardness Tester, EPMA™-8050G Electron Probe Microanalyzer, DTG-60 TG/DTA Simultaneous Measuring Instrument, TMA-60 Thermomechanical Analyzer

Multifaceted Evaluation of EV Drive Motor Shaft Produced by Radial Forging

Fumiaki Yano, Takuo Ono, Mana Oshiro, Atsuko Naganishi

User Benefits

◆ Improvement of processing technology and material strength can be expected by multifaceted analysis of hollow shafts manufactured by radial forging.

◆ Evaluation of the mechanical properties of metal materials is possible by the precision universal testing machine and hardness tester.

◆ Evaluation of the elemental distribution measurement and phase transformations related to improvement of the strength of metal materials is possible by EPMA and thermal analysis.

■ Introduction

Moves to achieve carbon neutrality to reduce greenhouse gas (GHG) emissions have accelerated in recent years. As part of this trend, the shift to electric vehicles (EVs) in the automotive industry is playing a major role in realizing a decarbonized society. Since improvement of the cruising range is required for wider adoption of EVs, auto body weight reduction has been taken up as a development theme. Reduction of the weight of EV shafts is a particularly important issue for development, as it does not simply improve the vehicle cruising range, but is also expected to improve motor response by reducing inertia. Radial forging is an innovative forging technology of hollow shaft which makes it possible to form the outer and inner diameters of parts at the same time by applying force from the radial direction of hollow shafts or hollow axis with a hammer (die) while simultaneously inserting a core bar into the shaft to transcribe the inner diameter shape [1]. Hollow shafts produced by the radial forging process are attracting attention as next-generation shafts that satisfy both strength and weight reduction.

In addition to the evaluation of the mechanical properties of motor shafts by the static tensile test and hardness test described in previous reports [2,3], in this Application News, an elemental analysis using an electron probe microanalyzer (EPMA) and evaluation of thermal properties with thermal analysis instruments were newly conducted. This article introduces an example of a multifaceted evaluation of motor shafts comparing the results of various types of measurements, as shown in Table 1.

Table 1 Composition of this Article

Evaluation method	Content of evaluation
① Static tensile test	• Measurement of tensile strength, elastic modulus, and breaking elongation
② Hardness test	• Measurement of Vickers hardness
③ Measurement of elemental distribution	• Element mapping analysis • Comparison of tensile strength and element mapping analysis • Comparison of breaking elongation and element mapping analysis • Evaluation of local hardness measurement by hardness test and element mapping analysis
④ Evaluation of thermal properties	• Thermogravimetric and differential thermal analysis measurement (TG-DTA measurement) • Thermomechanical analysis (TMA measurement)

■ Static Tensile Test (Test Piece Information)

The test pieces were cut from four types of products, three of which were processed by radial forging and one which was not processed (Blank). The radial forging products were forged so that the reduction of cross-sectional area (reduction of area: RoA) was 50, 60, or 70 % relative to that of the Blank. Fig. 1 shows an image of the test piece sampling positions. The test pieces were cut from five positions from 4 to 28 mm from the product surface layer at intervals of 6 mm. However, the test pieces for the radial forging product with 70 % RoA were taken from four positions from 4 to 22 mm from the surface. Table 2 shows the test piece information.
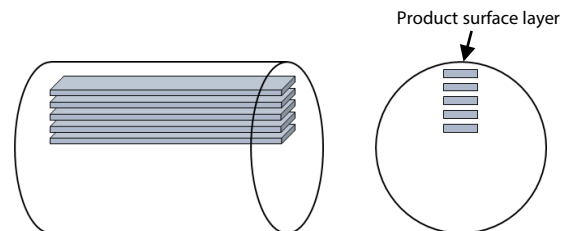

Fig. 1 Image of Test Piece Sampling Positions

Table 2 Test Piece Information

Test piece material	: SCr420
Test piece dimensions	: Thickness: 2.5 mm, width: 11 mm, length of parallel part: 56 mm
Types of test pieces	: Test piece ①: Blank Test piece ②: Radial forging (RoA: 50 %) Test piece ③: Radial forging (RoA: 60 %) Test piece ④: Radial forging (RoA: 70 %)
Test piece sampling positions	: 4, 10, 16, 22, 28 mm from surface * For test piece ④ only: 4, 10, 16, 22 mm

(Test material was provided by Tsuzuki Manufacturing Co., Ltd.)

■ Static Tensile Test (Measurement Results)

The tension test was carried out using a Shimadzu AGX-V precision universal testing machine. Fig. 2 shows the condition of the test. As can be seen in Fig. 2, a TRViewX non-contact digital video extensometer was mounted on the testing machine to measure the breaking elongation of the test piece. Fig. 3 shows the condition of the back side of a test piece. For accurate measurement of the elastic modulus and Poisson's ratio, the test was conducted with a biaxial strain gauge attached to the back side of the test piece. Table 3 shows the instrument configuration. The test conditions were set referring to JIS Z 2241 (Metallic materials – Tensile testing). Table 4 shows the test conditions. As one example of the test results, Fig. 4 shows the stress-strain curves of the test pieces ① and ②. Both test pieces were taken from the 4 mm position.
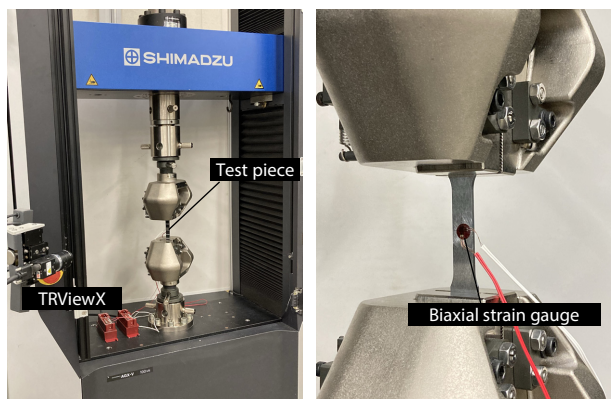

Fig. 2 Condition of Test

Fig. 3 Condition of Back Side of Test Piece

Table 3 Instrument Configuration

Precision universal testing machine	: AGX-V
Load cell	: 100 kN
Grip	: Non-shift wedge-type grip
Extensometer	: TRViewX120S
Software	: TRAPEZIUM™X-V

Table 4 Test Conditions

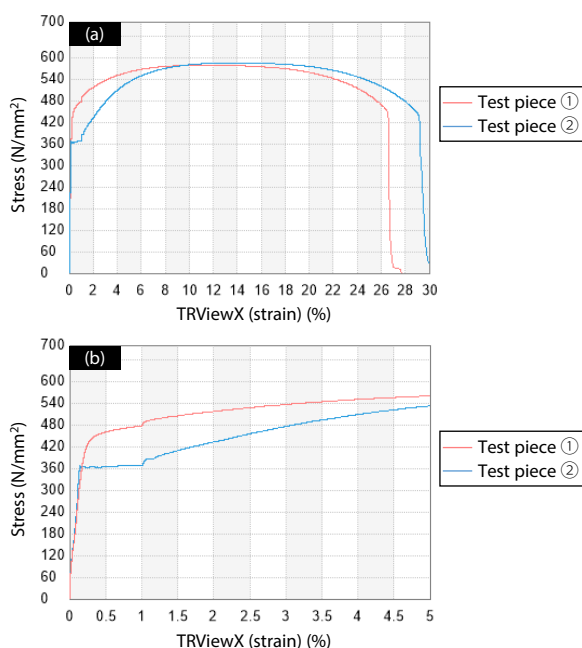|	
Test speed	: V1 10 MPa/s V2 5 %/min (switch to V2 at V2>V1) V3 40 %/min (switch at 1 % strain)
Gauge length	: 30 mm (TRViewX)
Number of tests	: n = 3

Fig. 4 Example of Stress-Strain Curves
(a) Entire Region of Test, (b) Initial Period of Test

As shown in Fig. 4, a yield point did not appear in test piece ①, which was the Blank material, but a yield point appeared in test piece ②, which was subjected to radial forging. Fig. 5 shows the various mechanical properties at each sampling position from the surface layer. Although there were differences in tensile strength and elastic modulus between the Blank and radial forging products, there were almost no differences depending on the test piece sampling positions. Poisson's ratio showed virtually constant values regardless of the test piece sampling position and whether radial forging was applied or not. Breaking elongation was also virtually constant for sampling positions up to a depth of 16 mm from the surface, regardless of whether radial forging was applied or not, but the breaking elongation of test pieces ② and ③ decreased at 22 mm and 28 mm. Thus, the forging region that displays excellent properties can be identified from these results.
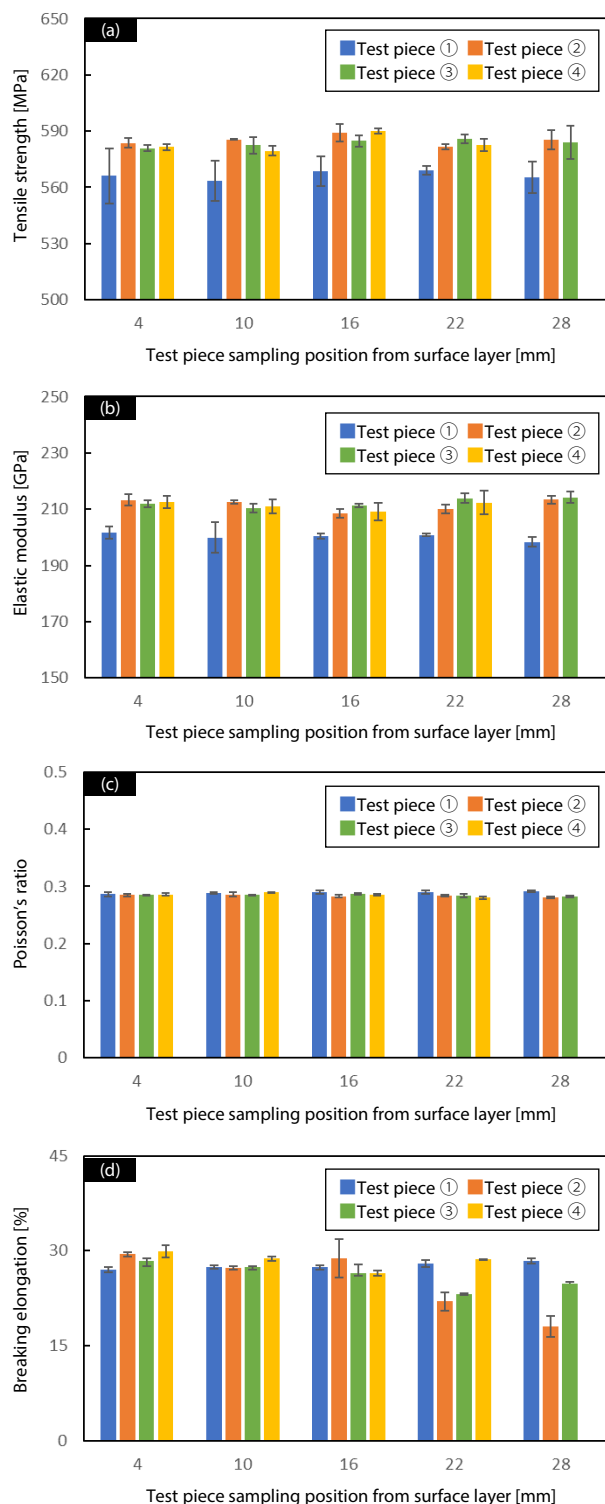

Fig. 5 Mechanical Properties at Test Piece Sampling Positions from Surface Layer
(a) Tensile Strength, (b) Elastic Modulus,
(c) Poisson's Ratio, (d) Breaking Elongation

■ Measurement of Vickers Hardness (Test Piece Information)

Fig. 6 (a) shows the sampling positions of the Blank, which is the test piece material before radial forging. The colored portion is cut from material with a cylindrical shape (shown by the dotted line). Fig. 6 (b) and (c) show the position from which four types of radial forging test pieces were cut out, consisting of one location with RoA of 50 % and three with RoA of 70 %. These specimens were mirror-polished, and Vickers hardness was measured at approximately 30 points at 1 mm intervals from the surface side along the lines shown by the red dotted lines in Fig. 6. Table 5 shows the measurement conditions. Fig. 7 is an image showing the measurement locations, which was photographed using the Stage View function of the hardness tester, and Fig. 8 is an example of an indentation image after the measurement.
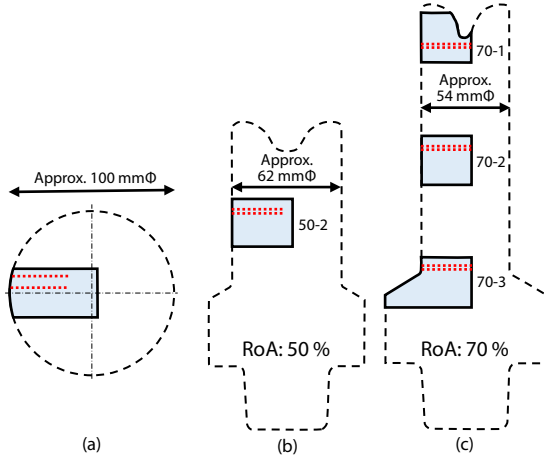
Fig. 6 Test Piece Sampling Positions and Measurement Positions
(a) Blank, (b) Radial Forging (RoA: 50 %) (c) Radial Forging (RoA: 70 %)

Table 5 Measurement Conditions

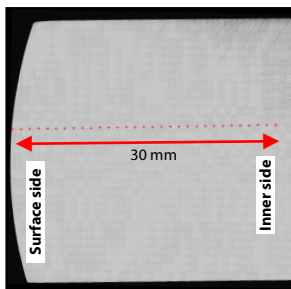|	
Hardness tester	: HMV-G31-FA series Micro Vickers hardness tester
Indenter type	: Micro Vickers indenter
Force	: HV 0.2 (1.96 N)
Holding time	: 10 s
Pitch and number of measurements	: 1 mm intervals, 29 or 30 points

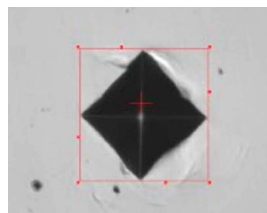Fig. 7 Image of Blank by Stage View Function

Fig. 8 Indentation Image (Blank, 2nd Indentation, 24th Point)

■ Measurement of Vickers Hardness (Measurement Results)

Fig. 9 to Fig. 13 show the hardness measurement results. Regarding the hardness distribution, the hardness of the Blank tended to be high near the surface, decreased toward the interior, and then become almost uniform from about 6 mm. In contrast, the hardness of the radial forging products 50-2 and 70-2 was substantially uniform regardless of the surface or interior measurement position. Comparing radial forging products with the same 70 % RoA, the variation of the measured values on the interior side at tip (70-1) and the root (70-3) tended to be large. The investigation of the factors in this is presented on p. 6, together with the results of the EPMA element mapping analysis.

Based on the results described above, although the hardness of the Blank tended to be high in the near-surface region, no large significant differences were observed in the hardness of the radial forging products due to the degree of forging processing (i.e., length of striking time in forging).
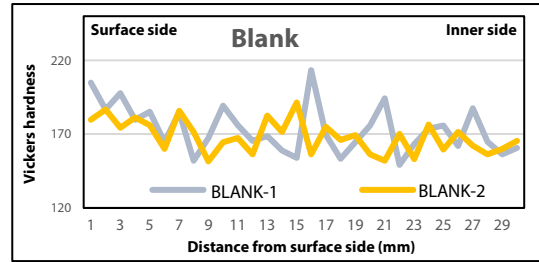

Fig. 9 Hardness Measurement Results of Blank
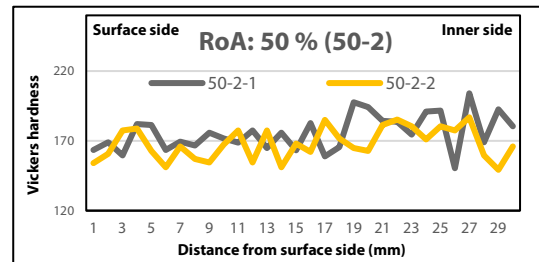

Fig. 10 Hardness Measurement Results of Radial Forging Product (50-2)
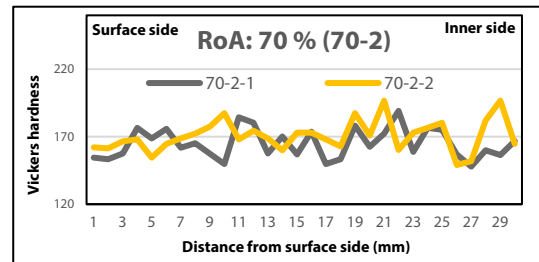

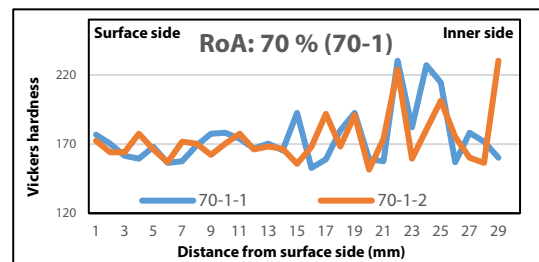Fig. 11 Hardness Measurement Results of Radial Forging Product (70-2)

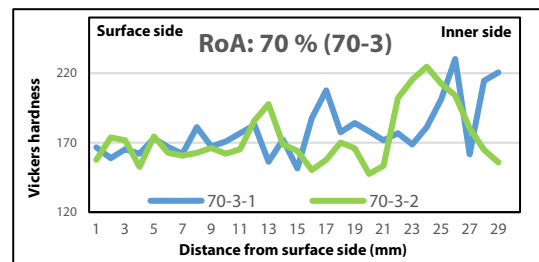Fig. 12 Hardness Measurement Results of Radial Forging Product (70-1)

Fig. 13 Hardness Measurement Results of Radial Forging Product (70-3)

■ Wide-Area Element Mapping Analysis by EPMA

A wide-area element mapping analysis was carried out along the indentation positions of the Blank and the 50 % and 70 % radial forging products (see Fig. 6) indented by the hardness tester. As one example, Fig. 14 shows a backscattered electron image (BEI) of the radial forging product with RoA of 50 % and the element mapping images of C, Si, Cr, Mn, and Fe, which are the main constituent elements. For C and Cr, which displayed especially distinctive distributions, Fig. 15 through Fig. 17 show enlarged element mapping images of the areas corresponding to 3 to 5 mm, 9 to 11 mm, 15 to 17 mm, 21 to 23 mm, and 27 to 29 mm from the surface side to the interior for the three types of test pieces. It should be noted that BEI is one type of SEM image, and expresses mainly the difference of the mean atomic numbers and surface topography information such as the crystal orientation and extreme irregularities (cavities caused by Vickers indentation) as differences in contrast. Element mapping images are color representations of the detected X-ray intensity, and as the intensity increases, the mapping image shows that the concentration of the element is relatively high at that position.

Looking at the distributions of the respective elements, in the radial forging products, flows of the component distribution along the direction (longitudinal direction) parallel to the surface are particularly apparent in the mapping images of Si, Cr, and Mn. It is thought that the crystals and microstructure of the material change in the process of radial forging, resulting in segregation of certain trace elements. Furthermore, the distribution of these elements is fine in the shallow region below the surface, while in the deeper region, the distribution becomes thick and there are large differences in shading. In addition, since the distribution is finer in the 70 % RoA material (70-2) than in the 50 % RoA material (50-2), it is thought that the crystal grain size and microstructure have changed as a result of a high degree of forging process (long striking time).

■ Observation of Fiber Flow

Chemical treatment was applied to the cross sections of equivalent test pieces of the radial forging products, and the fiber flow was observed. Fig. 18 shows the cross-sectional image of the RoA 50 % product, and undulations can be seen in the flow of the flow lines. Fig. 19 shows a higher magnification image of the tip portion overlaid with the EPMA element mapping image of Cr. Thus, it can be understood that the fiber flow and the flow of the element distribution of Cr are in good agreement.
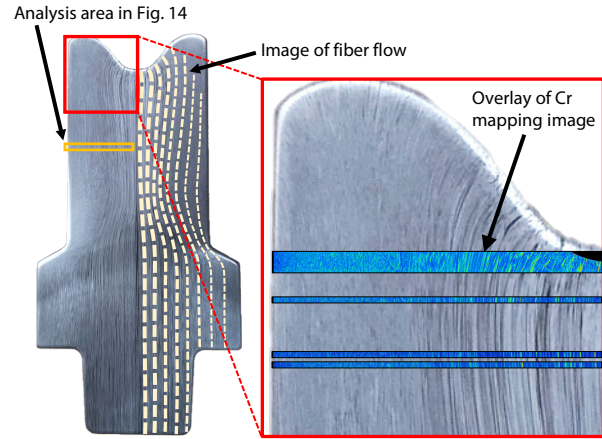

Fig. 18 Photograph of Fiber Flow Observation of Cross Section of 50 % RoA Product

Fig. 19 Overlay of Enlargement of Fiber Flow Observation Image and Element Mapping Image of Cr
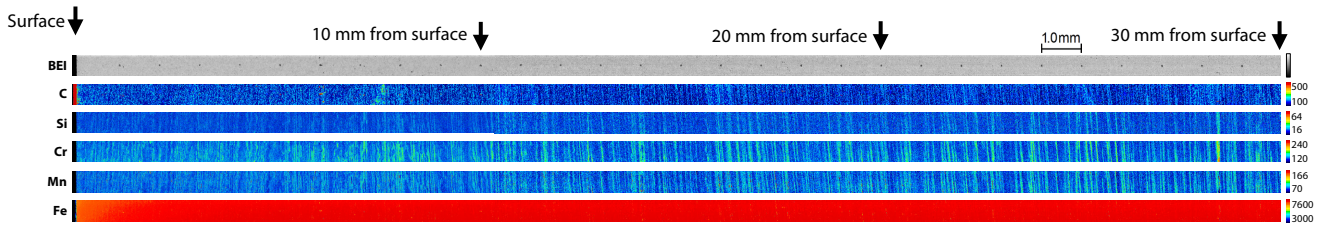

Fig. 14 Wide-Area Element Mapping Images (50-2)
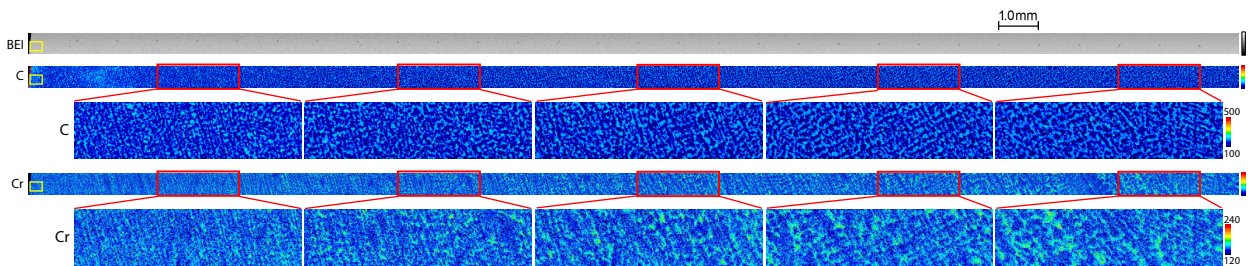

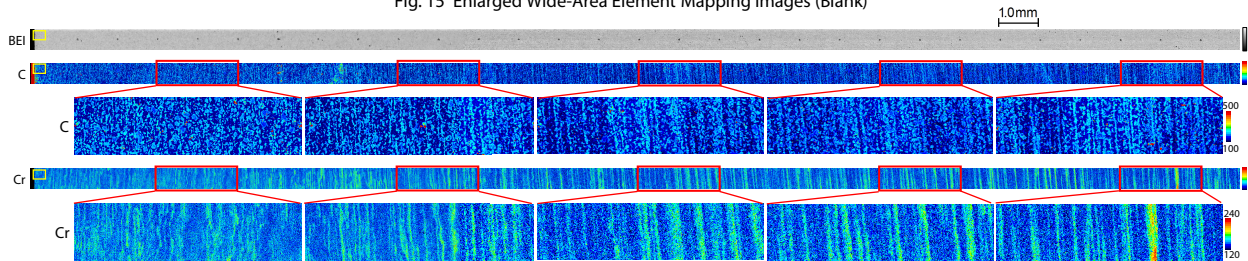Fig. 15 Enlarged Wide-Area Element Mapping Images (Blank)

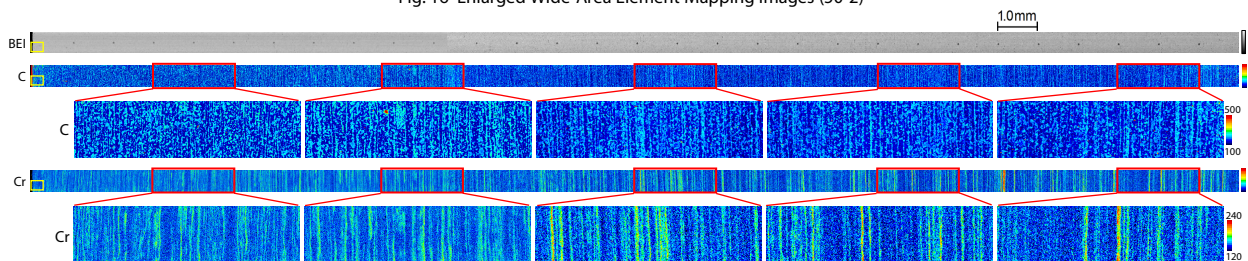Fig. 16 Enlarged Wide-Area Element Mapping Images (50-2)

Fig. 17 Enlarged Wide-Area Element Mapping Images (70-2)

■ Narrow-Area Mapping Analysis by EPMA

A narrow-area mapping analysis was carried out for the near-surface region of the Blank and the radial forging products (RoA: 50 %, 70 %). Fig. 20 shows enlarged mapping images of the near-surface region in Figs. 15 to 17 on the previous page, and Fig. 21 shows enlarged mapping images of the areas in the frames in Fig. 20. In the BEI, images reflecting the crystal orientation were acquired by channeling contrast, and it can be seen that the crystal grain size has been refined by radial forging. Looking at the distribution of Cr, a flow of the composition distribution along the direction parallel to the surface (longitudinal direction) clearly appears in the radial forging products, and a fine distribution can be observed,

particularly in the 70 % product. In the distribution of C in Fig. 20, in comparison with the 50 % radial forging product, the microstructure in which C has precipitated tends to be small in the 70 % radial forging product. In the enlarged view in Fig. 21, a fine lamellar structure (pearlite; a microstructure separated into the two phases of ferrite (α Fe) and cementite (Fe_3C)) can be seen, and as the radial forging processing time becomes longer, the spacing between these layers shows a tendency to become narrower, suggesting that the strength of the material increases.

For a detailed example of an evaluation of the micro precipitates, please refer to the separate report [4].
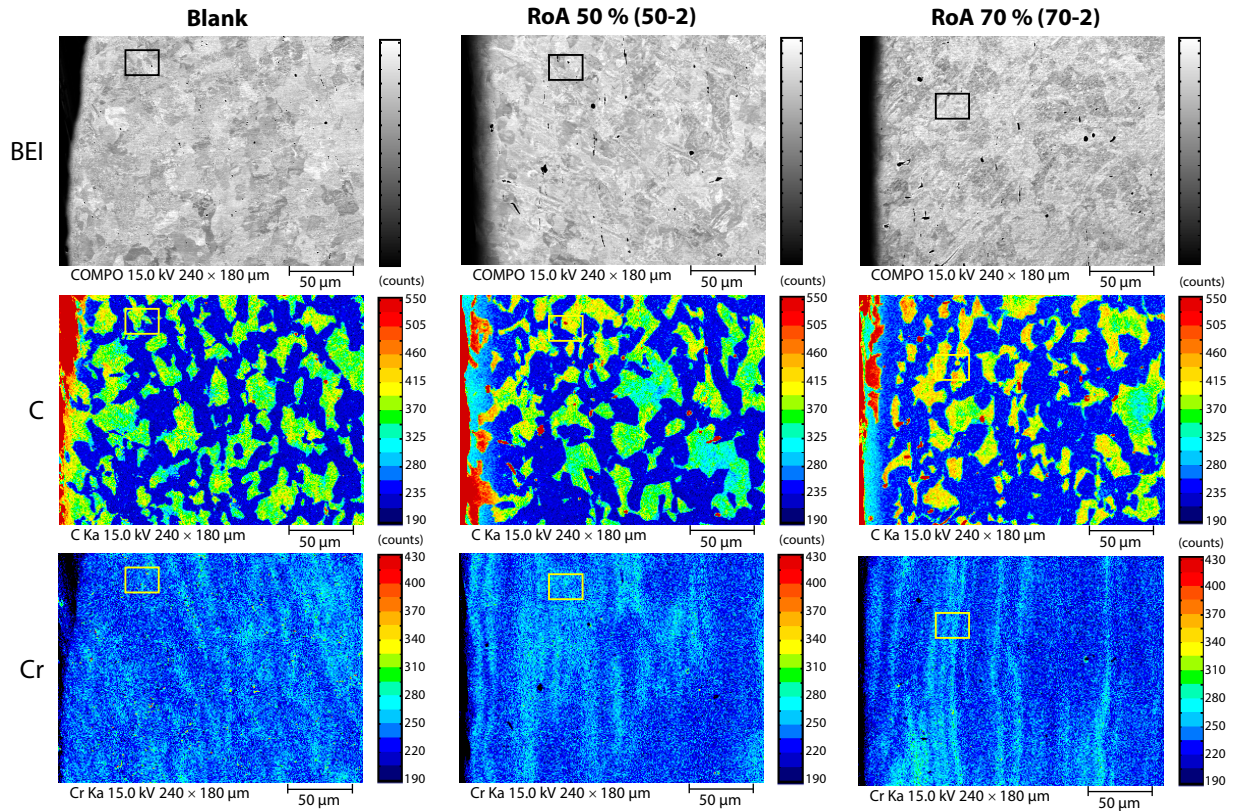

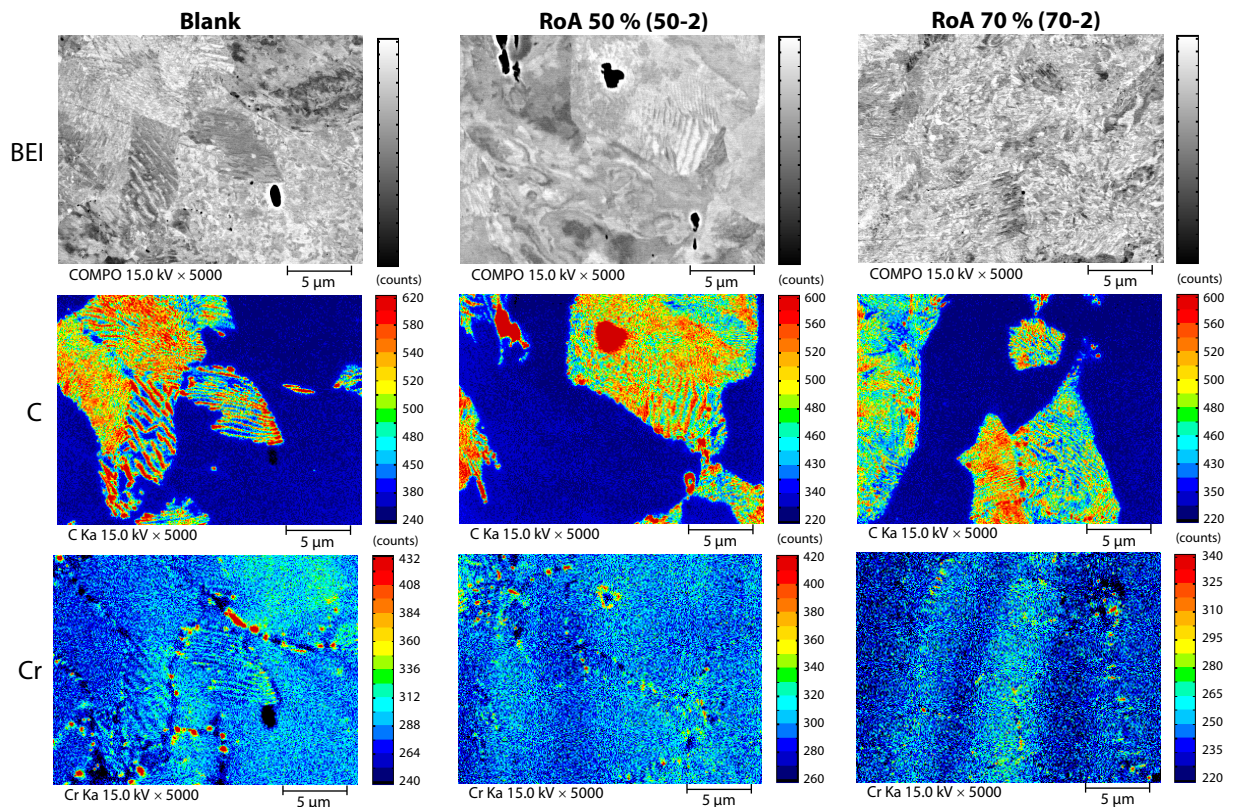Fig. 20 Element Mapping Images of Near-Surface Region (Enlargements of Yellow Frames in Figs. 15 to 17)

Fig. 21 Elemental Mapping Images of Near-Surface Region (Enlargements of Frames in Fig. 20)

Comparison of Tensile Strength and Element Mapping Analysis

From the tensile strength results of the static tensile test (Fig. 5 (a)), the tensile strength of the radial forging products is higher than that of the Blank. Based on the results of the element mapping analysis by EPMA (pp. 4-5), it is considered that the strength of the radial forging products increased as a result of refinement of the microstructure and crystal grain size.

Comparison of Breaking Elongation and Element Mapping Analysis

In the results for breaking elongation in the static tensile test (Fig. 5 (d)), the breaking elongation value of the 50 % RoA radial forging product, i.e., test piece ②, showed a tendency to decrease toward the interior side. This is thought to occur because the weak part of the material fractures easily under tension, as the fiber flow in the 50 % RoA material is not parallel to the direction of the tensile test, but rather, tends to be curved in a wavy pattern depending on the location, as can be understood from the EPMA element mapping analysis (Fig. 14, Fig. 16) and the photographs of the fiber flow (Fig. 18, Fig. 19). However, a decrease in mechanical properties in the product interior can be ruled out as a possible factor because the aimed product shape in this experiment was hollow.

Evaluation of Local Hardness Measurements by Hardness Test and Element Mapping Analysis

Comparing radial forging products with the same 70 % RoA, a tendency toward large variations in the measured values on the interior side was seen at the tip (70-1) and root (70-3). To investigate the factors in this difference, a mapping analysis of the indentation area was carried out using EPMA[3]. As one example, Fig. 22 shows the mapping images (secondary electron image (SEI) and element mapping of C) of a position where the surrounding area of the test piece surface around an indentation displayed a poor shape. The areas of strain, which appears in the form of wrinkles around the indentation, can be seen in the SEI. These areas correspond to parts with a low X-ray intensity of C, while the areas where strain did not occur tend to have a high X-ray intensity of C. It is thought that this wrinkle-like strain behavior occurred due to differences in hardness caused by segregation of C.

Next, the distribution of various elements in the test piece with 70 % RoA (70-1) was investigated. Fig. 23 shows the hardness distribution (the same figure is also shown in Fig. 12). Here, we focused on points where the hardness measurement value was large (24 mm) and small (20 mm). Fig. 24 and Fig. 25 show the element mapping analysis results. Fig. 24 and Fig. 25 show enlarged views of the results for C and Cr on the interior side (19 to 25 mm from the surface) and in the area around the indentations, respectively. As can be seen here, the X-ray intensities of C and Cr are low around the indentation at the depth of 20 mm, and high around the indentation at 24 mm. These results suggest that the hardness measurement values were influenced by segregation of C and/or Cr.

From the above, it was found that strain could be seen in the area around cavities caused by indentation during the hardness test, and when the variations in the measured values of hardness was large, mainly segregation of C is considered to be the cause. Conversely, this also implies that the degree of segregation of elements can be estimated from the size of variations in the measured values of hardness.
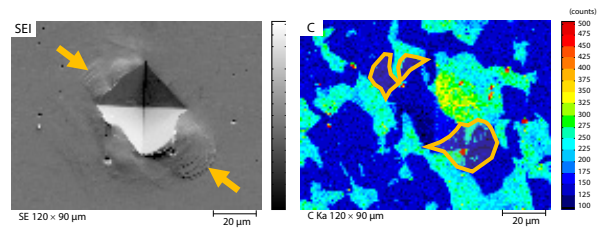

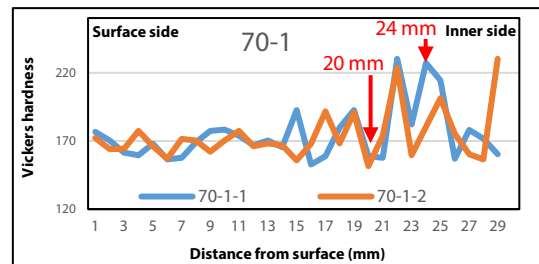Fig. 22 Elemental Mapping Images of Indentation Cavity with Poor Shape

Fig. 23 Hardness Measurement Results of Radial Forging Product (RoA: 70 %; 70-1)
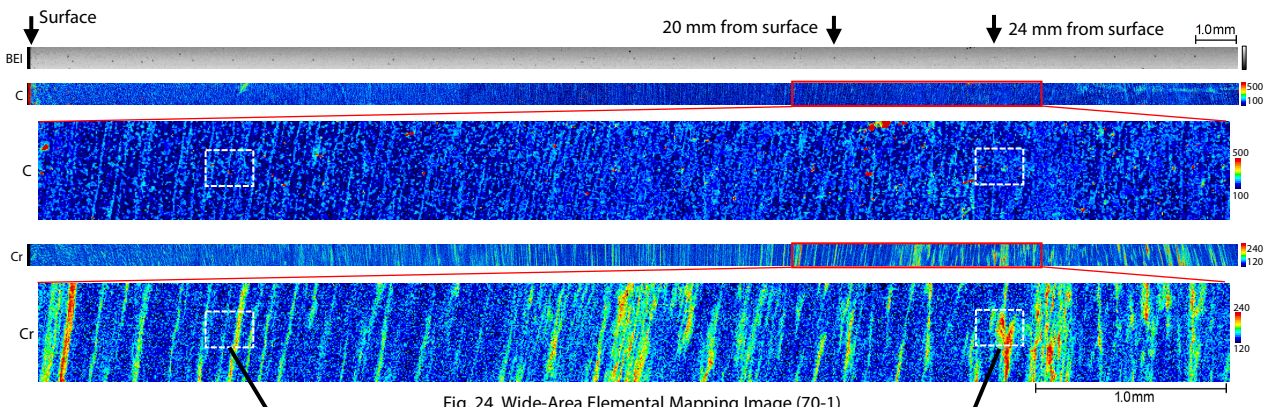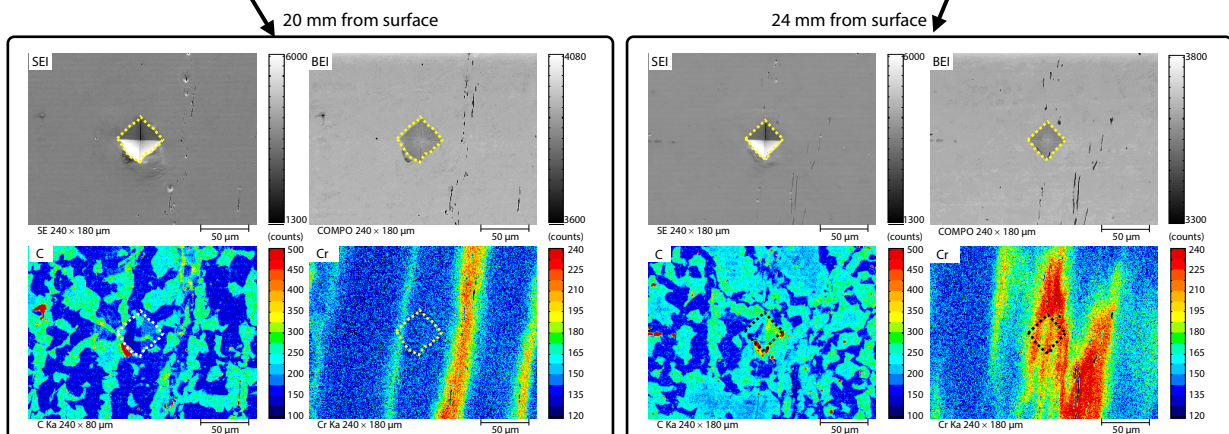

Fig. 24 Wide-Area Elemental Mapping Image (70-1)

Fig. 25 Enlarged Mapping Images of Frames in Fig. 24 (70-1)

■ TG-DTA Measurement of Radial Forging Products

Two types of radial forging products made with SCr 420 were measured using DTG -60 in Fig. 26 under the measurement conditions shown in Table 6. In comparison with the 50 % RoA material, additional hammer force was applied to the 70 % RoA material to obtain a test material with a large degree of working. Table 7 shows the results of measurements (n = 2) of the respective materials. According to Fig. 28 and Fig. 29, no weight change was observed from 200 ˚C to 1000 ˚C, and an endothermic peak was seen at around 770 ˚C.

Fig. 26 DTG-60   Fig. 27 TMA-60

Table 6 TG-DTA Measurement Conditions

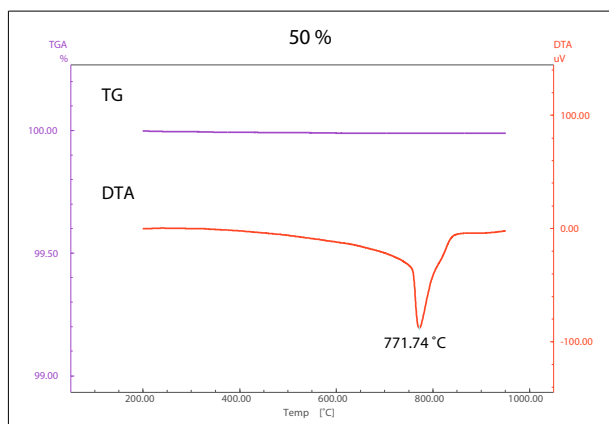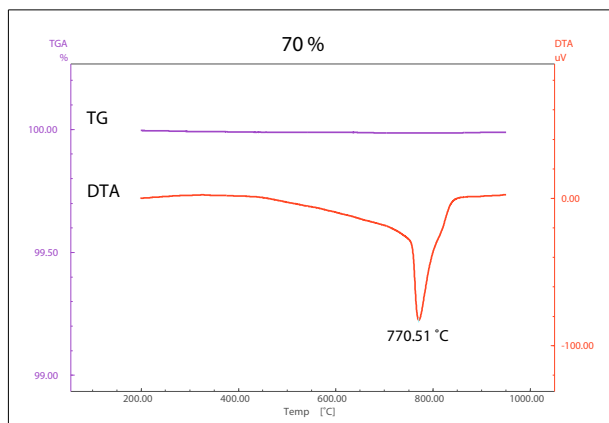|	
Instrument	: Simultaneous Thermal Analysis DTG-60
Sample weight	: 392 mg (approx.)
Cell	: Alumina macrocell
Atmosphere	: Nitrogen
Heating rate	: 20 ˚C/min

Fig. 28 TG-DTA Curve of 50 % RoA Material

Fig. 29 TG-DTA Curve of 70 % RoA Material

Table 7 TG-DTA Measurement Results

Sample name	Peak (˚C)
50 %_①	771.7
50 %_②	771.6
50 %_Ave.	771.6
70 %_①	770.5
70 %_②	770.4
70 %_Ave.	770.5

■ TMA Measurement of Radial Forging Products

The 70% RoA material was measured using TMA-60 in Fig. 27 under the measurement conditions shown in Table 8. Since an inflection point could be seen at around 790 ˚C in the TMA curve in Fig. 30, the endothermic reaction detected in the TG-DTA curve is thought to be a peak due to phase transformation. Since the microstructure is homogenized by forging at temperatures higher than the transformation temperature and refined by forging at temperatures lower than the transformation temperature, if the transformation temperature can be determined, it will be possible to establish the line between homogenization and refinement of the microstructure.

Table 8 TMA Measurement Conditions

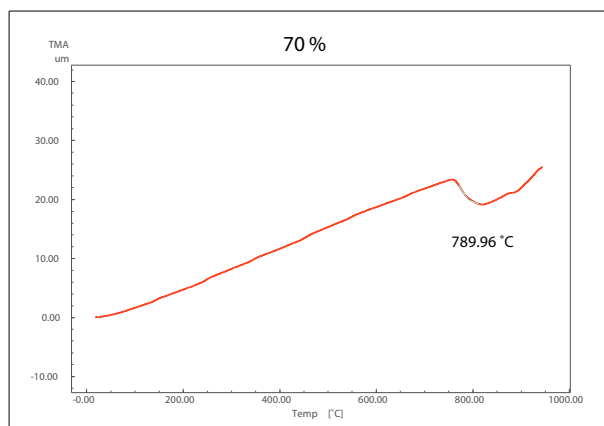|	
Instrument	: Thermomechanical analyzer TMA-60
Sample length	: 2.592 mm
Initial LOAD	: 10 g
Atmosphere	: Nitrogen
Heating rate	: 10 ˚C/min

Fig. 30 TMA Curve of 70 % RoA Material

■ Comparison of Evaluation of Thermal Properties and Element Mapping Analysis

From the TG-DTA measurement results, the endothermic peak top temperature of the 70 % RoA material was lower than that of the 50 % RoA material. Furthermore, the results of the element mapping analysis by EPMA (Fig. 16, Fig. 17, Fig. 20, Fig. 21) confirmed that the microstructure of the 70 % RoA material became finer as a result of working (forging). Based on these facts, the 70 % RoA material, which has a higher degree of processing, has a finer grain structure in the ferrite + pearlite phase due to processing, and the endothermic peak top temperature is thought to be lower because the reaction occurs faster.

■ Summary of Comparison between Blank and Radial Forging Products

In the evaluation of mechanical properties by the precision universal testing machine, improvement could be seen in the measured values of tensile strength and the elastic modulus of the radial forging products, while the value of Poisson's ratio was substantially constant. On the other hand, it was found that the breaking elongation of the radial forging products decreased in the interior side.

In the Vickers hardness measurements, a difference in the hardness of the surface and interior of the Blank was observed, but the hardness of the radial forging products was almost constant. However, there were conspicuous variations in the measured values of the hardness of the radial forging products at the ends of the forged products in the direction of elongation by forging, and it was suggested that this was due to the effect of segregation of elements (mainly C) in the material.

From the element mapping analysis by EPMA, flows of the composition distribution (mainly of Si, Cr, and Mn) along the direction perpendicular to the striking direction in forging were observed, and these composition flows coincided with the flows seen in the observation of the fiber flow. In addition, an element mapping analysis of microregions also revealed that precipitation of finer crystal grains occurred as the degree of working by forging increased.

In the evaluation of thermal properties, weight change was not observed in the radial forging products from 200 °C to 1,000 °C, and an endothermic peak was seen at around 770 °C. From the TMA measurement results, it was found that this endothermic reaction is a peak due to phase transformation. Moreover, even when both products were subjected to radial forging, it was found that the endothermic peak top temperature was lower in the specimen with 70 % RoA, which was a larger degree of working. When considered in combination with the results of the element mapping analysis by EPMA, it is thought that the phase transformation to ferrite + pearlite in the process of cooling during radial forging, and further crystal grain refinement by the effect of forging, were factor in this decrease in the endothermic peak top temperature.

As described above, it was possible to confirm the effectiveness of radial forging by a multifaceted evaluation using various testing, measurement, and analysis instruments.

■ Multifaceted Evaluation by Various Testing, Measurement, and Analysis Instruments

As described in this article, it is possible to carry out a multifaceted evaluation of materials and products by measuring their mechanical properties with a precision universal testing machine (Fig. 31), measuring Vickers hardness with a hardness tester (Fig. 32), measuring the elemental distribution and observing the crystal orientation by EPMA (Fig. 33), and measuring the weight change and endothermic reaction by thermal analysis (Fig. 34, Fig. 35). These instruments can also be expected to provide evaluation tools for evaluating the processed regions that display excellent properties, and for optimizing forging processing conditions and heat treatment control conditions.

Fig. 31 AGX-V Precision Universal Testing Machine

Fig. 32 HMV-G31-FA Micro Vickers Hardness Tester

Fig. 33 EPMA-8050G Electron Probe Microanalyzer

Fig. 34 DTG-60   Fig. 35 TMA-60

<References>

1) Tsuzuki Manufacturing Co., Ltd., Introduction of Shaft
   https://www.tsuzuki-mfg.co.jp/solution/2020/01/post-12.php

2) Application News 01-00440-EN, "Evaluation of Electric Vehicle (EV) Motor Shafts Produced by Radial Forging: Radial Forging Processing Affects Static Tensile Characteristics"

3) Application News 01-00445-JP, "Evaluation of EV Drive Motor Shaft by Radial Forging Process —Confirmation of Correlation between Hardness Distribution and Element Distribution—"

4) Application News 01-00513-EN, "Evaluation of EV Drive Motor Shaft Produced by Radial Forging: Elemental Mapping Analysis by EPMA"

AGX, HMV, and EPMA are trademarks of Shimadzu Corporation or its affiliated companies in Japan and/or other countries.

SHIMADZU

Shimadzu Corporation

www.shimadzu.com/an/

LIKE

Click like if you enjoyed this application.